J Solid State Electrochem (2010) 14:1855–1861
DOI 10.1007/s10008-010-1066-0

ORIGINAL PAPER

Inhibitor effect of sodium benzoate on the corrosion behavior of nanocrystalline pure iron metal in near-neutral aqueous solutions

Vahid Afshari · Changiz Dehghanian

Received: 14 November 2009 / Revised: 28 March 2010 / Accepted: 30 March 2010 / Published online: 28 April 2010

Abstract Nanocrystalline iron coating was produced on carbon steel surface by pulse electrodeposition using citric acid bath. The grain size of a nanocrystalline surface was analyzed by X-ray diffractometry and scanning electron microscopy. The electrochemical behavior of nanocrystalline iron coating in the presence of sodium benzoate was evaluated in 30 mg l^{-1} NaCl + 70 mg l^{-1} Na_2SO_4 aqueous solution using potentiodynamic polarization curves and electrochemical impedance spectroscopy. The results were compared with that of the coarse-grained iron surface. The thermodynamic properties of the inhibitor adsorption were also determined. The results indicated that corrosion inhibition of sodium benzoate in near-neutral aqueous solution was increased as the grain size of iron was decreased from micro- to nanocrystalline surface. This was reported in terms of excess free energy of nanocrystalline surface.

Keywords Nonocrystalline iron · Corrosion · Inhibitor · Polarization · EIS

Introduction

Nanostructured materials may be defined as those materials whose structural elements—clusters, crystallites, or molecules—have dimensions in the 1- to 100-nm range [1–3]. The ultrafine crystallite structure of nanocrystalline materials, due to a large fraction of atoms located in the interface region, causes significant improvements in selected mechanical, physical, and chemical properties compared to their coarse-grained counterparts [4, 5]. Nanocrystallization of a coarse-grained polycrystalline material provides a new approach to the improvement of properties without changing its chemical composition. The nano grain size and the high volume fraction of grain boundaries may result in corrosion behaviors different from that of polycrystalline materials. Lorenz and co-workers [6–8] showed that the kinetics of iron dissolution depended on the substructure of the electrode material. The influence of crystal imperfections on the reaction kinetics was established by comparing studies of iron sample by X-ray analysis and electron microscopy with electrochemical steady-state and transient measurements. These findings were confirmed by other authors [9, 10]. Youssef and co-workers reported that nanocrystalline Zn coatings exhibited an improved corrosion resistance in comparison to electrogalvanized steel in NaOH solution [11]. Our studies have also demonstrated that nanocrystalline iron coating prepared by electrodeposition offers superior corrosion resistance in alkaline solution [12]. Rofagha and co-workers investigated the corrosion behavior of nanocrystalline pure nickel coating and compared that with polycrystalline pure nickel coating in H_2SO_4 media. They reported that the nanocrystalline coating showed a higher current density in the passive region, resulting in higher corrosion rates [13, 14]. The corrosion behavior of the nanostructured alloy $Cu_{90}Ni_{10}$ in neutral solution containing chlorides indicated a decrease in the protective properties of the passive layer [15]. For the nanocrystalline Co coatings, researches have shown that grain size reduction has a little effect on the overall corrosion performance of Co coatings in Na_2SO_4 solution [16]. These reports demonstrate that the effect of nano-

V. Afshari (✉) · C. Dehghanian
Department of Metallurgy and Materials Engineering,
Faculty of Engineering, University of Tehran,
P.O. Box 11155-4563, Tehran, Iran
e-mail: vafshari@ut.ac.ir

C. Dehghanian
e-mail: cdehghan@ut.ac.ir

structure surface on corrosion behavior varies among metal systems and corrosion environments. The first mechanism action of inhibitor is adsorption onto metal surface which is influenced by the surface charge of metal, inhibitor structure, and the type of electrolyte [17]. The impetus of this work was to evaluate the effect of sodium benzoate on corrosion inhibition of nanocrystalline iron coating and its grain size reduction in comparison to that of micro iron grain size coating in near-neutral aqueous solution. The corrosion behavior of samples was evaluated by potentiodynamic polarization and ac impedance spectroscopy.

Experimental

The nanocrystalline iron coating was produced on carbon steel surface via pulse electrodeposition technique using an experimental setup described elsewhere [12]. Coarse-grained specimen was prepared by high-temperature annealing of pure iron (99.99%) at 1,050 °C for 3 h in inert atmosphere followed by furnace cooling. The surface microstructure and grain size of the annealed and as-received samples were examined by optical microscopy. The grain size of the nano-grained specimen was analyzed by X-ray diffractometry (XRD) and scanning electron microscopy (SEM). X-ray diffraction studies were carried out using a Philips X'Pert-Pro instrument operated at 40 kV and 30 mA with CoK_{α} radiation (λ=0.1789 nm) at a scan rate of 0.05° s^{-1}.The full width at half-maximum of the peak is broadened due to grain size reduction. The most intensive first-order peak (110) of the XRD patterns was taken for detailed analysis using a Gaussian fitting curve. The average grain size, D, was estimated according to the Scherrer equation [18]:

$$D = 0.9\lambda/\beta\cos\theta \quad (1)$$

where D is the average grain size, λ is the wavelength of the X-ray, θ is the Bragg angle for the peak, and β is the intrinsic (true) profile full width at half-maximum intensity (FWHM). The β parameter was calculated using the Gaussian–Gaussian (GG) relationship:

$$\beta^2_{\exp} = \beta^2 + \beta^2_{inst} \quad (2)$$

where $\beta_{\exp}$ and β_{ins} are the full width of the diffraction line measured at FWHM of experimental and instrumental

Table 1 Treatment conditions and average grain size of various specimens

Specimen	Conditions	Grain size (μm)
As-cast Fe	As-recieved	20
Annealed Fe	Annealed at 1,050 °C for 3 h	300
Nano Fe	Electrodeposited	0.045

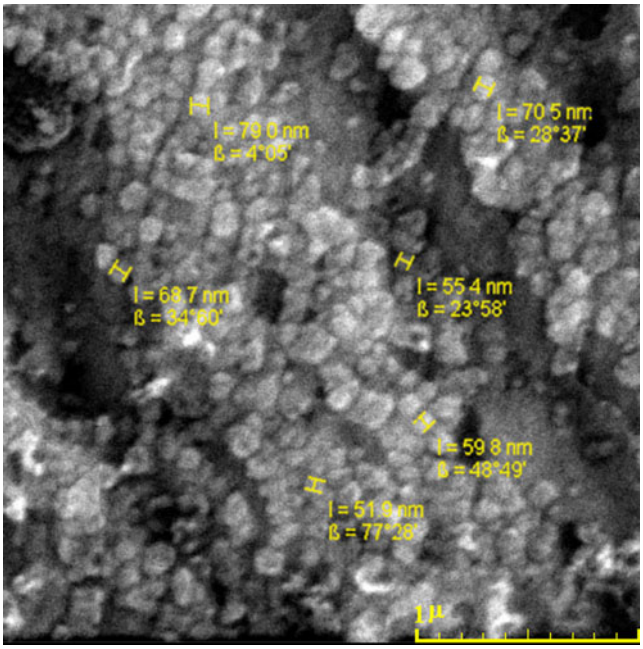

Fig. 1 SEM of nanocrystalline Fe deposit

profiles, respectively. The annealed iron with an average grain size of 300 μm was used as reference sample to determine instrumental broadening corrections. The treatment conditions and average grain sizes of the specimens are summarized in Table 1. Electrochemical measurements were made in 30 mg l^{-1} NaCl + 70 mg l^{-1} Na_2SO_4 aqueous solution prepared from analytical-grade chemical and distilled water. All chemical solutions were freshly prepared and the temperature of the solutions during measurements was kept at 25 °C. The electrochemical measurements were made with a conventional three-electrode cell. A saturated calomel electrode (SCE) was used as a reference electrode. The auxiliary electrode was a platinum foil with a total surface area of 2 cm^2. Working electrodes were specimens with iron nanocrystalline surface, as received and annealed with a

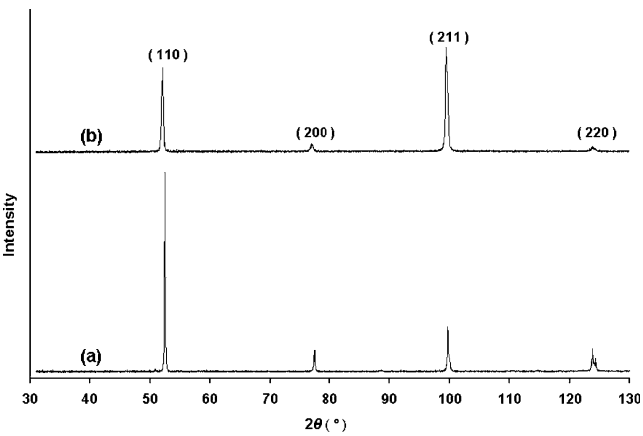

Fig. 2 XRD patterns of (**a**) annealed and (**b**) nanocrystalline Fe specimens

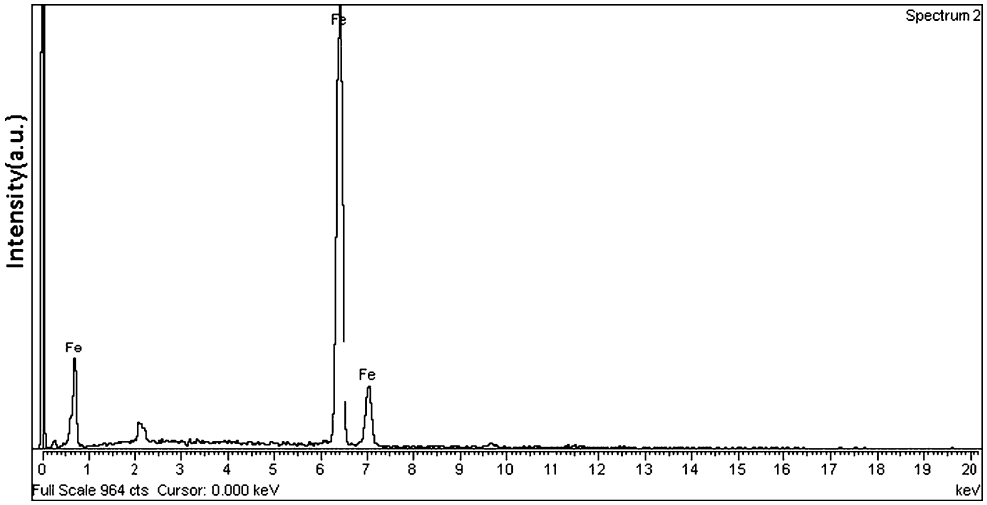

Fig. 3 EDS result of nanocrystalline Fe deposit

coarsed grain size. The specimen's surface area was selected to be 2.25 cm^2. Electrochemical impedance spectroscopy (EIS) measurements were conducted at an open circuit potential after immersion of a sample into the solution for 30 min. The applied potential amplitude was chosen to be 5 mV with frequency ranging from 100 KHz to 0.01 Hz. The collected data were analyzed with an equivalent circuit using "ZView2" software. Potentiodynamic polarization curves were used to determine the corrosion potential ($E_{corr.}$) and corrosion current density ($I_{corr.}$). The samples were polarized from 0.25 V_{SCE} beyond the corrosion potential to an anodic potential of 1 V_{SCE} beyond the corrosion potential with a scan rate of 1 mV s^{-1} using potentiostat MODEL 273 (EG&G) with "Softcorr 352" software. Prior to measurements, the working electrode was allowed to stabilize in the electrolyte for 1 h. Potential versus current density characteristics of the specimens were monitored. All polarization measurements were carried out after EIS measurements. All measurements were repeated for at least two times. The surface morphology and microstructure of the nanocrystalline deposited layer were examined using a scanning electron microscope and their compositions were analyzed using an X-ray energy dispersive spectrometer (EDS) attached to the SEM.

Results and discussion

Figure 1 shows the SEM image of iron nanocrystalline coating sample. The uniform ultrafine grains were mostly equiaxed crystallites interconnected by incoherent interfaces. Figure 2 shows the XRD patterns of the annealed iron sample and nanocrystalline iron coating produced by pulse electrodeposition. For the nano-grained surface specimen, the width of the peaks was significantly broadened due to the ultrafine grain size (45 nm). The crystallographic texture was changed from a strong (110) fiber texture to a (110) (211) double-fiber texture for pulse-plated iron nanocrystals. The grain size as obtained by XRD (Fig. 2) presents an average value for the surface layer, while the SEM image only presents the grains at a particular location. The chemical composition of the electrodeposited iron was determined using EDS. The iron content in the electrodeposited iron nanocrystalline coating was ~100 at. wt% measured by EDS (Fig. 3).

Potentiodynamic polarization curves for the different specimens in 30 mg l^{-1} NaCl + 70 mg l^{-1} Na_2SO_4 solution are shown in Figs. 4 and 5. The corrosion parameters were extracted from the polarization curves using a commercial software (Model 352) and summarized in Table 2. It was found that the corrosion current density was changed significantly as the microstructure morphology was changed. These results indicated that the addition of sodium benzoate to corrosive solution made polarization curves to exhibit more noble corrosion potentials and, furthermore, it lowered the corrosion rate with a decrease in grain size. This behavior was probably due to the more inhibitor

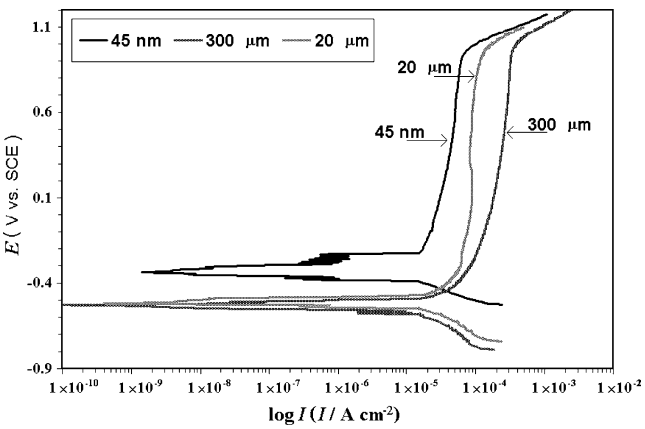

Fig. 4 Potentiodynamic polarization curves of iron of different grain sizes in 30 mg l^{-1} NaCl + 70 mg l^{-1} Na_2SO_4 + 0.4 mol l^{-1} sodium benzoate

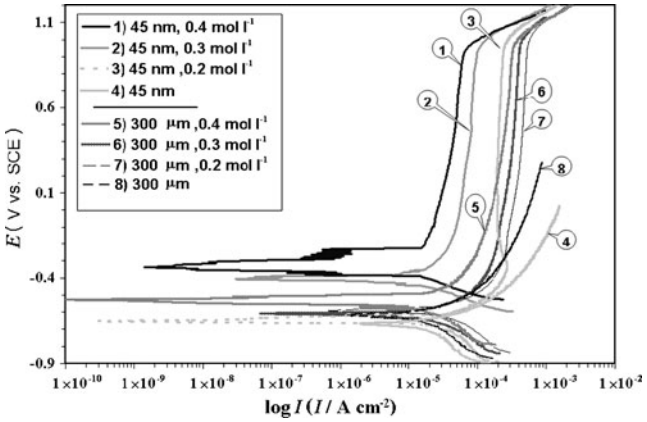

Fig. 5 Potentiodynamic polarization curves of iron of different grain sizes in 30 mg l^{-1} NaCl + 70 mg l^{-1} Na_2SO_4 + 0~0.4 mol l^{-1} sodium benzoate

adsorption and formation of a passive film on the metal surface. The passive film caused a barrier effect for charge transfer of anodic reactions and markedly decreased the corrosion rate. This lower current density was attributed to a higher grain boundary area and triple junction content in the nanocrystalline specimen [19], which provided different sites for electrochemical activities. However, the difference in current density diminished at higher potentials (1.1 V_{SCE}) at which the overall dissolution rate was overwhelmed with the structure-controlled dissolution rate which was observed at lower potentials. The negative shift in the open circuit potential for the nanocrystalline specimens in the absence of an inhibitor was assumed to be due to the presence of more active atoms on the nanostructured surface which have taken part in the reaction and produced a high corrosion rate in the nanocrystalline iron-coated surface. As it was anticipated, sodium benzoate changed the kinetics of the cathodic process but the positive shift in the open circuit potential was reflected by the anodic action of the inhibitor system. In the presence of sodium benzoate, the metal surface formed a diffusion barrier layer composed of reaction products on the surface, which was referred to as a passive film. The passivating effect of sodium benzoate in the presence of oxygen is due to the fact that the anion of benzoic acid $C_6H_5COO^-$ forms a strong chemical bond with iron via carboxyl groups, which reduces the free energy of the system and impedes the passage of ion–atom of iron from the lattice into the solution. This lowers the reactivity of a considerable number of the iron atoms on the surface and facilitates passivation of the remaining atoms by oxygen of water. The resistance of this film to dissolution is related to their physical and chemical nature, which determines the corrosion resistance of the metal.

The adsorption behavior of a corrosion inhibitor is a major factor for its inhibition properties. The adsorption of an inhibitor species, I, on an electrode surface in aqueous solutions may be considered as a place for the following exchange reaction:

$$I_{sol} + n(H_2O)_{ads} = I_{ads} + n(H_2O)_{sol} \quad (3)$$

where n is the number of water molecules displaced by one inhibitor molecule. The displacement of pre-adsorbed water molecules by adsorbing inhibitor molecules may be considered as a fundamental step of inhibition. The ability of an inhibitor to replace water molecules depends on the electrostatic interaction between the metal and the inhibitor. The interaction was first started on the surface of crystalline lattice defects and nanocrystal materials which have a high density of grain boundaries and dislocations inside the grains [20]. The grain boundaries in nanocrystalline materials are usually not in a state of equilibrium; this may result in a larger driving force for passive film formation [21]. The intercrystalline volume represents a region of stored excess energy with respect to the bulk of a grain. This may cause a significant driving force for the blocking of surface sites for anodic dissolution. This may be due to the anion of benzoic acid which exerts a force on nanocrystalline materials. The excess free energy (G_{excess}) per unit volume of a nanocrystalline solid has the form:

$$G_{excess} = \alpha d^{-1} + \beta d^{-2} + \gamma d^{-3} \quad (4)$$

where d is the grain diameter, α, β, and γ are constants incorporating geometrical factors, α is proportional to the grain boundary excess free energy per unit area, β is related to the junction energy per unit length, and γ is related to the vertex energy [22]. The large specific surface area of

Table 2 Corrosion potential (E_{corr}), corrosion current density (I_{corr}), and inhibitor efficiency (%IE) in 30 mg l^{-1} NaCl + 70 mg l^{-1} Na_2SO_4 + C mol l^{-1} sodium benzoate aqueous solutions

Specimen	C ($mol l^{-1}$)	E_{corr} (V vs. SCE)	I_{corr} ($\mu A cm^{-2}$)	IE %	Specimen	C ($mol l^{-1}$)	E_{corr} (V vs. SCE)	I_{corr} ($\mu A cm^{-2}$)	IE %
Nanocrystalline Fe deposit	—	-0.687	26.91	—	Annealed Fe	—	-0.633	19.06	—
Nanocrystalline Fe deposit	0.2	-0.639	13.49	49.8	Annealed Fe	0.2	-0.587	14.79	22.4
Nanocrystalline Fe deposit	0.3	-0.376	10.47	61.1	Annealed Fe	0.3	-0.584	12.88	31.4
Nanocrystalline Fe deposit	0.4	-0.276	8.32	69.1	Annealed Fe	0.4	-0.538	11.84	37.9
As cast Fe	—	-0.653	23.44	—	As cast Fe	0.4	-0.492	10.96	53.2

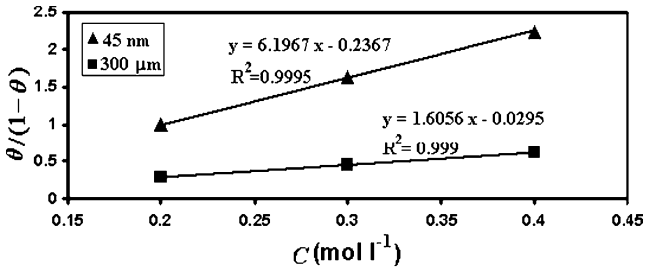

Fig. 6 Langmuir adsorption isotherm plots of iron of different grain sizes in 30 mg l^{-1} NaCl + 70 mg l^{-1} Na_2SO_4 + C mol l^{-1} sodium benzoate

nanocrystalline and concomitantly large specific surface energy cause the surface-sensitive properties (like catalytic activity) to be enhanced [23–26] and the process where the surface energy is the driving force are facilitated [27–29]. Hence, it is believed that the nanocrystal electrodeposited iron coating has a high density of active sites for inhibitor adsorption. This may lead to a high fraction of passive layers and low corrosion rates. In order to describe the nature and the strength of adsorption, the experimental data have been fitted to a series of adsorption isotherms and the best fit was obtained with the use of Langmuir adsorption isotherm (Fig. 6). The Langmuir adsorption isotherm can be expressed as [30]:

$$C/\theta = 1/K + C \tag{5}$$

where θ is a fractional coverage of the metal surface, C is the inhibitor concentration in the electrolyte, and K is the equilibrium constant for the adsorption/desorption process and it is related to the standard free energy of adsorption $\left(\Delta G^{\ominus}_{ads}\right)$ according to [31]:

$$K = 1/55{:}5\exp\left(-\Delta G^{\ominus}_{ads}/RT\right) \tag{6}$$

where R is the universal gas constant and T is the absolute temperature. The value of $\Delta G^{\ominus}_{ads}$ was found to be −14.16 and −10.89 kJ mol^{-1} for the nanocrystalline (45 nm) and the coarse grain size (300 µm) iron, respectively. The high negative values of $\Delta G^{\ominus}_{ads}$ indicate that these compounds are strongly adsorbed on the iron surface. It is usually accepted that the values of $\Delta G^{\ominus}_{ads}$ around −20 kJ mol^{-1} or lower than that are indicative of the electrostatic attraction between the charged metal surface and the charged organic molecules in the bulk of the solution [32]. Hence, it is believed that the nanocrystal electrodeposited iron coating has a high density of active sites for inhibitor adsorption. This may lead to a high fraction of passive layers and low corrosion rate. All EIS curves in Fig. 7 show only one capacitive loop, which indicate that charge transfer is the major controlling factor. The corrosion kinetics parameters such as R_{ct} and C_{dl} were obtained from the ac impedance data using an appropriate model (ZView2 software). The results are presented in Table 3. The circuit includes the solution resistance, R_s, in series with one RC (time constant), τ=R_{ct}.CPE, representing the resistance and constant phase element (CPE) of the passive film. In the mathematical analysis modelling of the

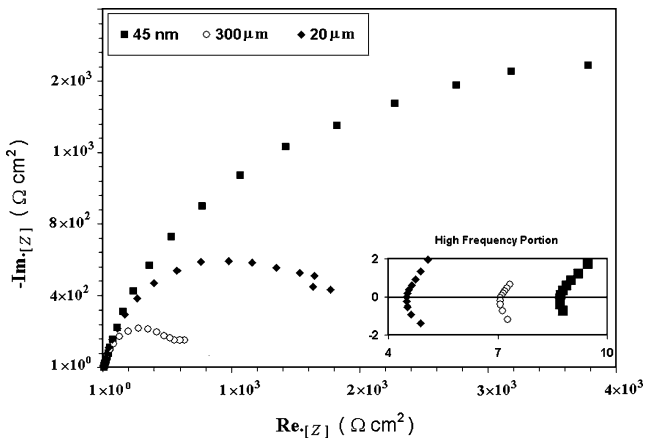

Fig. 7 Complex plane plots of iron of different grain sizes in 30 mg l^{-1} NaCl + 70 mg l^{-1} Na_2SO_4 + 0.4 mol l^{-1} sodium benzoate

Table 3 Impedance parameter values in 30 mg l^{-1} NaCl + 70 mg l^{-1} Na_2SO_4 + 0.4 mol l^{-1} sodium benzoate

Specimen	R_s (Ω)	R_{ct} (Ω cm^2)	C_{dl} (µF)
Nanocrystalline Fe deposit	8.717	4841	551.42
Annealed Fe	7.127	631	951.14
As-cast Fe	5.511	1780	607.15

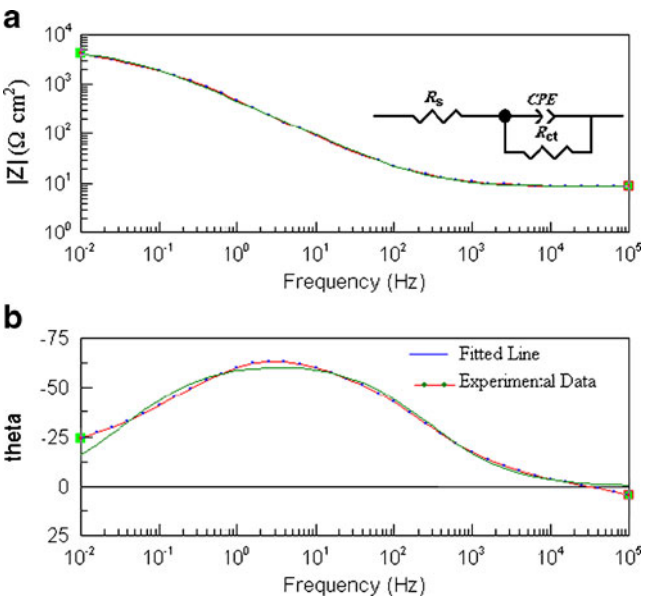

Fig. 8 A comparison between experimental impedance data for nanocrystalline Fe deposit (45 nm) in 30 mol l^{-1} NaCl + 70 mol l^{-1} Na_2SO_4 + 0.4 mol l^{-1} sodium benzoate aqueous solution and the results of analysis with ZView2 . Bode graphs (**a**) magnitude and (**b**) phase angle vs. frequency

impedance data, a CPE was substituted for the capacitive behavior in order to do a better fit of the depressed semicircles due to microscopic fluctuations of the surface because of the inhomogeneous surface of the electrode [33]. The impedance of a constant phase element is given as follows:

$$Z_{\mathrm{CPE}} = 1/Qs^{\alpha f} \tag{7}$$

where Q is the CPE parameter, αf is the CPE exponent (phase shift), $s=\mathrm{i}\omega$ and ω is the angular frequency ($\omega=2\pi f$, where f is the AC frequency), and i here is the imaginary unit. When the value of αf is 1, the CPE behaves like an ideal double-layer capacitance (C_{dl}) [34–37]. The correction of capacity to its real values is calculated from:

$$C_{\mathrm{dl}} = Q(\omega_{\max})^{\alpha f - 1} \tag{8}$$

where $\omega_{\max}$ is the frequency at which the imaginary part of impedance ($-Z_{\mathrm{i}}$) has a maximum value [38].

A typical comparison of the experimental and the fitted data in the Bode plot was displayed in Fig. 8. It can be seen that the simulated curve basically follows the experimental data at the most of frequency measurements. Therefore, the experimental data are suitably fitted with the equivalent circuit embedded in Fig. 8. It was found that the charge transfer impedance was increased as the double layer capacitance was decreased with the gradual reduction of iron grain size. This may be due to a decrease in local dielectric constant and/or an increase in the thickness of the electrical double layer, suggesting that the active sites of nanostructure surfaces promote the adsorption of the benzoic acid anions and hence increasing the degree of coverage on iron surface. These results are in good agreement with the results obtained from polarization measurements shown in Table 2.

Conclusions

Based on the results obtained from this research, the following conclusions can be drawn:

1. A lower current density, a more noble potential, and a lower corrosion rate were found for nanocrystalline iron surfaces in comparison to the microcrystalline iron surfaces.
2. The nanocrystal electrodeposited iron coating had a high density of nucleation sites for encouraging the adsorption of benzoate ions, which leads to a high fraction of passive layers and low corrosion rates.
3. The excess free energy per unit volume of a nanocrystalline solid caused the surface-sensitive properties to be enhanced and processes where the surface energy is the driving force are facilitated.
4. The standard free energy of adsorption for iron in the solution of 30 mg l^{-1} NaCl + 70 mg l^{-1} Na_2SO_4 with sodium benzoate became more negative as the grain size was decreased from the submicrocrystalline to the nanocrystalline.
5. Electrochemical impedance spectroscopy results indicated that, for the nanocrystalline structure surfaces, the charge transfer resistance in the presence of an inhibitor was reasonably increased and its capacitances were decreased when it was compared to the coarse morphological surfaces. This may be attributed to a decrease in local dielectric constant or an increase in the thickness of the electrical double layer.

References

1. Gleiter H (1982) Mater Sci Eng 52:91–131
2. Gleiter H (1995) Z Metall 86:78–83
3. Gleiter H (2000) Acta Mater 48:1–29
4. Thiele E, Klemm R, Hollang L, Holste C, Schell N, Natter H, Hempelmann R (2005) Mater Sci Eng A 390:42
5. Yang B, Vehoff H, Hempelmann R (2006) Int J Mater Res 97:1220
6. Lorenz WJ, Eichkon G (1965) J Electrochem Soc 112:1225
7. Lorenz WJ, Eichkon G, Bunsenges Ber (1966) Phys Chem 70:99
8. Eichkon G, Lorenz WJ, Albert L, Fischer H (1968) Electrochim Acta 13:183
9. Eichkon G, Lorenz WJ (1968) Z Metalloberflache 22:102
10. Lorenz WJ (1968) Das elektrochemische Verhalten des aktiven Reineisens in sauren Lösungen. Universitat Karlsruhe, Habilitationsschrift
11. Youssef Kh MS, Koch CC, Fedkiw PS (2004) Corros Sci 46:51
12. Afshari V, Dehghanian C (2009) Corros Sci 51:1844–1849
13. Rofagha R, Langer R, El-Sherik AM (1991) Scripta Metall Mter 25:2867
14. Rofagha R, Splinter SJ, Erb U (1994) Nanostruct Mater 4:69
15. Barbucci A, Farne G, Mattaezzi P, Riccieri R, Cereisola G (1999) Corros Sci 41:463
16. Kim SH, Aust KT, Erb U, Gonzalez F, Palumbo G (2003) Scripta Mater 48:1379
17. Rozenfeld IL (1981) Corrosion Inhibitor. McGraw-Hill, New York
18. Cullity BD (1978) Elements of X-ray Diffraction, 2nd edn. Addison-Wesley, Reading, pp 281–285
19. Surayanarayana C, Mukhopadhayay D, Patanker SN, Froes FH (1992) J Mater Res 7:2114
20. Balyanov A, Kutnyakova J, Amirkhanova NA (2004) Scripta Mater 51:225
21. Czerwinski F, Li H, Megret M, Szpunar JA, Clark DG, Erb U (1997) Scripta Mater 37:1967
22. Greer AL (1993) Mechanical properties and deformation behavior of materials having ultra-fine microstructures. Springer, New York, pp 53–77
23. Daniel MC, Astruc D (2004) Chem Rev 104:293–346
24. Lopez N, Norskov JK (2003) Abs Paper Am Chem Soc 225: U688–U688
25. Sommer WJ, Crne M, Weck M (2007) The ACS J Surf Colloids 23(24):11991–11995
26. Zhai S, Zhang Y, Shi X, Wu D, Sun YH, Shan Y, He MY (2004) Catal Lett 93:225–229
27. Bowen P, Carry C (2002) Powder Technol 128:248–255

28. Goujon C, Goeuriot P (2001) Mater Sci Eng A 315:180–188
29. Nihara K (1991) J Cream Soc Jpn 99:974–982
30. Agrawal R, Namboodhiri TKG (1990) Corros Sci 30:37
31. Ateya BG, Anadoli EEL, El-Nizamy FM (1984) Corros Sci 24:509
32. Moretti G, Quartarone G, Tassan A, Zlngales A (1996) Electrochim Acta 41
33. Nihara K, Ronbunshi NSKG (1999) J Cream Soc Jpn 99:974–982
34. Popova A, Sokolova E, Raicheva S, Christov M (2003) Corros Sci 45:33
35. Gohr H, Schaller J, Schiller CA (1993) Electrochim Acta 38:1961
36. Kliskic M, Radosevic J, Gudic S, Katalinic V (2000) J Appl Electrochem 30:823
37. Babic Samardzija K, Hackerman N (2006) Anti Corros Method Mater 53:19
38. Mohana KN, Badiea AM (2008) Corros Sci 50:2939–2947